Effects of Partial Substitution of Mo^{6+} by Cr^{6+} and W^{6+} on the Crystal Structure of the Fast Oxide-Ion Conductor Structural Effects of W^{6+}

G. Corbel,[†] Y. Laligant,[†] F. Goutenoire,[†] E. Suard,[‡] and P. Lacorre*[,†]

Laboratoire des Oxydes et Fluorures, UMR CNRS 6010, Université du Maine, 72085 Le Mans Cedex 9, France, and Institut Laue-Langevin, BP 156, 38042 Grenoble Cedex 9, France

Received January 19, 2005. Revised Manuscript Received May 28, 2005

The crystal structure of the solid solutions $La_2Mo_{2-y}Cr_yO_9$ ($y \leq 0.5$) and $La_2Mo_{2-y}W_yO_9$ ($y \leq 1.4$) has been studied using X-ray and neutron powder diffraction. These two series of lanthanum molybdates, which belong to the LAMOX family of fast oxide-ion conductors, exhibit a different structural behavior depending on the substituting element. The Cr series follows a regular Vegard-type evolution of crystallographic parameters. However, the behavior of the W series is different, the lattice constant varying in a nonlinear fashion with substitution level, resulting in a smaller cell volume for higher tungsten contents, despite the larger ionic radius of tungsten. Two main structural effects are evidenced: a variation in the distribution of ligands around tungsten, made apparent through the changing balance of oxygen O2 and O3 site occupancies along the series, and a nonlinear evolution of interatomic distances and angles involving the O1 oxygen site. An alternative structural description, based on [O1La_3Mo] anti-tetrahedra, is proposed in order to better account for the transport properties of these materials.

1. Introduction

Research in the field of fast oxide-ion conductors is very active, fostered by the current development of solid oxide fuel cells and need for electrolytes working at intermediate temperature. Our recent discovery of a new family of fast oxide-ion conductors, called LAMOX and derived from $La_2Mo_2O_9$,[1,2] has triggered further works on these compounds. Among them, Tarancón et al. reported recently[3] that $La_2Mo_2O_9$ compares favorably, as a pure ionic conductor under low oxygen pressure, to Gd-substituted CeO_2 (CGO), the state-of-the-art material in the field of intermediate temperature solid electrolytes.[4] However, hexavalent molybdenum oxides usually suffer degradation in a highly reducing atmosphere as already reported on $La_2Mo_2O_9$ itself,[5] which questions the aging behavior of this compound under such stringent conditions. We have shown in a previous paper that molybdenum substitution by tungsten has a beneficial effect on the stability of the compound in reducing conditions.[6] The substitution range is wide (up to around 80%), and moreover tungsten suppresses the phase transition by stabilizing the β form at room temperature. Therefore, the tungsten series appears to be the most promising in terms of structural stability for applications.

In a precedent work on the LAMOX family, we observed an unusual evolution of the cubic cell parameter in the series $La_2Mo_{2-y}W_yO_9$ (see Figure 7 of ref 2), later on confirmed by Collado et al.[7] Despite the slightly larger size of tungsten compared to molybdenum, a decrease of the crystal cell parameter was observed above a certain substitutional range. The cell parameter evolution upon substitution did not seem to follow the current Vegard's law commonly observed in the other cubic members of the LAMOX family.

In the current paper we use neutron scattering in order to address the issue of the tungsten series' crystal structure with aim to detect any significant change upon substitution, which would give a coherent explanation for the abnormal cell parameter evolution. For a general survey on the influence of substitution by the transition elements belonging to the Mo column of the periodic table and a comparison with the effect of W substitution, the synthesis and crystal structure of the $La_2Mo_{2-y}Cr_yO_9$ series are also presented here.

2. Experimental Section

2.1. Synthesis. Due to the toxicity of hexavalent chromium, only small amounts (~1 g) of powder samples of $La_2Mo_{2-y}Cr_yO_9$ ($y =$ 0.1, 0.2, 0.3, 0.4, 0.5, 0.6) were prepared according to the following procedure. Stoichiometric powder mixtures of elementary oxides La_2O_3, MoO_3, and Cr_2O_3 spread over the bottom of an alumina boat were first heated at 500 °C for a night in a pure oxygen gas flow. The samples were then fired twice at 825 °C in the alumina boat under pure oxygen, for about 2 days each time with an intermediate grinding.

* To whom correspondence should be addressed. E-mail: philippe.lacorre@univ-lemans.fr.
[†] Université du Maine.
[‡] Institut Laue-Langevin.

(1) Lacorre, P.; Goutenoire, F.; Bohnke, O.; Retoux, R.; Laligant, Y. *Nature* **2000**, *404*, 856.
(2) Goutenoire, F.; Isnard, O.; Suard, E.; Bohnke, O.; Laligant, Y.; Retoux R.; Lacorre, P. *J. Mater. Chem.* **2001**, *11*, 119.
(3) Tarancón, A.; Norby, T.; Dezanneau, G.; Morata, A.; Peiró, F.; Morante, J. R. *Electrochem. Solid-State Lett.* **2004**, *7*, A373.
(4) Ivers-Tiffée, E.; Weber, A.; Herbstritt, D. *J. Eur. Ceram. Soc.* **2001**, *21*, 805.
(5) Goutenoire, F.; Retoux, R.; Suard, E.; Lacorre, P. *J. Solid State Chem.* **1999**, *142*, 228.
(6) Georges, S.; Goutenoire, F.; Laligant, Y.; Lacorre, P. *J. Mater. Chem.* **2003**, *13*, 2317.
(7) Collado, J. A.; Aranda, M. A. G.; Cabeza, A.; Olivera-Pastor, P.; Bruque S. *J. Solid State Chem.* **2002**, *167*, 80.

10.1021/cm0501214 CCC: $30.25
Published on Web 08/05/2005

Table 1. Ionic Radii[12] of Hexavalent Transition Elements in the VIA Column of the Periodic Table as a Function of Their Coordination Number (CN)

element	CN	ionic radius (Å)
Cr^{6+}	IV	0.26
	VI	0.44
Mo^{6+}	IV	0.41
	V	0.50
	VI	0.59
W^{6+}	IV	0.42
	V	0.51
	VI	0.60

Two series of powder samples of $La_2Mo_{2-y}W_yO_9$ where prepared, the first one in small amounts (2−2.5 g) for preliminary X-ray analysis and the second one in larger batches (30−40 g) for neutron diffraction measurements. All these samples where first heated at 500 °C for 12 h and then at higher temperature for 3 days. For some compositions, and especially for the large batches, after grinding, an additional firing for 3 days at the same or higher temperature was necessary in order to get pure samples. The final heating temperatures were, for the first series, 950 °C ($y = 0.3$), 1000 °C ($y = 0.5$ and 1.0), 1050 °C ($y = 1.2$), 1100 °C ($y = 1.5$), and 1150 °C ($y = 1.6$), and for the second series 950 °C ($y = 0.25$), 1000 °C ($y = 0.5$ and 0.75), 1050 °C ($y = 1.0$ and 1.2), and 1100 °C ($y = 1.4$).

2.2. Thermal Analysis. A differential thermal analysis (DTA) was performed in air on a ∼48 mg sample of $La_2Mo_{1.9}W_{0.1}O_9$, using a simultaneous DTA-TGA SDT 2960 apparatus (TA Instruments) with a heating/cooling rate of 20 °C·min^{-1}.

2.3. Structural Characterization. X-ray diffraction data were recorded on SIEMENS D500 (phase purity) and on BRUKER AXS D8 (structural analysis) Bragg−Brentano diffractometers (Cu Kα radiation). Neutron diffraction patterns were recorded on the Debye−Scherrer diffractometer D2B of the Institut Laue-Langevin (Grenoble, France). Long run diffractograms for structure determination were collected using the following conditions: for the Cr series X-ray patterns, 34 s/step of 0.02° in the [15°−130°] range, for the W series X-ray patterns, dusted through a 63 μm sieve, 43 s/step of 0.02 in the [14°−124°] range, and for the W series neutron patterns (wavelength 1.593641 Å, ∅15 mm vanadium container), in the [−7.45°−162°] range, with step 0.05°. The Rietveld program FullProf[8] was used for full-pattern matching and structural refinements, and the Diamond software[9] was used to draw the crystal structure.

3. Results and Discussion

3.1. Substitution of Molybdenum by Chromium. Within the synthesis conditions detailed above, the substitution range of molybdenum by chromium extends up to 25% Cr, namely, $La_2Mo_{1.5}Cr_{0.5}O_9$. Above this chromium amount, an impurity phase appears, identified as being $LaCrO_3$. In pure compounds, the samples color is a good indication of the oxidation state of chromium. Materials are yellow in the whole $La_2Mo_{2-y}Cr_yO_9$ series, testifying that chromium is at the +6 oxidation state (lower oxidation states of chromium usually give green or violet oxides, or darker if mixed valence).

All the studied compositions of the series ($y = 0.1$, 0.2, 0.3, 0.4, 0.5) have a cubic symmetry (space group $P2_13$).

(8) Rodriguez-Carvajal, J. *Physica (Amsterdam)* **1993**, *192B*, 55.
(9) DIAMOND−Visual Crystal Structure Information System, CRYSTAL IMPACT, Postfach 1251, D-53002 Bonn.

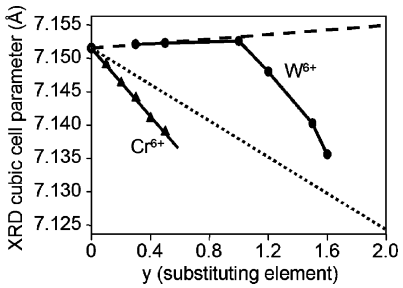

Figure 1. Crystal cell parameter evolution upon substitution of molybdenum by chromium (triangles) and tungsten (ovals) in $La_2Mo_2O_9$. Dashed and dotted lines correspond to linear extrapolations (see text for details) assuming tungsten has the same coordination number as molybdenum (dashed) or one ligand less (dotted).

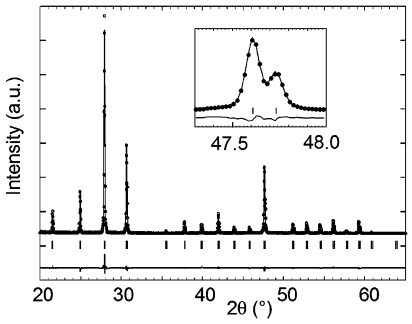

Figure 2. Rietveld fit of the $La_2Mo_{1.6}Cr_{0.4}O_9$ X-ray diffraction pattern with the structural model given in Table 2. In insert: detail showing the single (123) cubic reflection line (Cu $K\alpha_1+\alpha_2$ wavelength) usually broadly split in the monoclinic distortion of the α form.

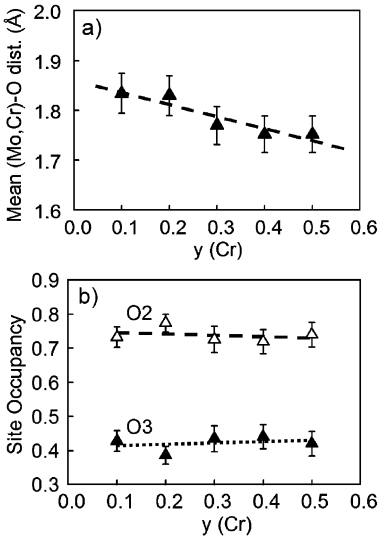

Figure 3. Decrease of the mean weighed (Mo,Cr)−O distance (a) and stability of oxygen sites occupancy (b) as a function of the chromium content y in $La_2Mo_{2-y}Cr_yO_9$ (dashed and dotted lines = linear regressions).

Hexavalent chromium being much smaller than hexavalent molybdenum (see Table 1), a reduction of the crystal cell volume is expected upon substitution by chromium. The cell parameter evolution along the series reflects this trend (see Figure 1) with a linear dependence on y, thus following the usual Vegard's law.

Due to the toxicity of hexavalent chromium, we have limited our structural analysis to X-ray diffraction, which requests a much lower sample amount than neutron diffraction. The drawback is that the localization of light atoms, such as oxide ions in our case, is less accurate. Table 2 gives the results of refinements in terms of atomic positions and

Table 2. Refined Crystal Structure Parameters (Space Group $P2_13$) in the Series $La_2Mo_{2-y}Cr_yO_9$ from X-ray Powder Diffraction Data

y		0.1	0.2	0.3	0.4	0.5
a (Å)		7.1490(1)	7.1463(1)	7.1441(1)	7.1410(1)	7.1389(1)
La (4a)	x	0.8547(2)	0.8525(2)	0.8526(2)	0.8525(2)	0.8529(2)
	occupancy	1	1	1	1	1
	B_{iso} (Å^2)	4.7(5)	4.2(4)	4.5(4)	4.3(3)	4.5(4)
Mo/Cr (4a)	x	0.1668(3)	0.1663(3)	0.1667(3)	0.1677(2)	0.1678(2)
	occupancy	0.95/0.05	0.9/0.1	0.85/0.15	0.8/0.2	0.75/0.25
	B_{iso} (Å^2)	5.5(1)	5.6(9)	5.4(8)	5.3(7)	5.3(7)
O1 (4a)	x	0.310(1)	0.321(1)	0.319(1)	0.316(1)	0.318(1)
	occupancy	1	1	1	1	1
	B_{iso} (Å^2)	7	7	7	7	7
O2 (12b)	x	0.975(2)	0.984(2)	0.984(2)	0.992(2)	0.993(2)
	y	0.199(2)	0.224(2)	0.209(2)	0.208(1)	0.205(1)
	z	0.359(2)	0.373(2)	0.361(2)	0.367(2)	0.361(2)
	occupancy	0.73(1)	0.77(1)	0.72(1)	0.72(1)	0.74(1)
	B_{iso} (Å^2)	7	7	7	7	7
O3 (12b)	x	0.841(3)	0.849(5)	0.900(3)	0.906(3)	0.911(3)
	y	0.592(4)	0.621(6)	0.683(3)	0.676(3)	0.683(3)
	z	0.555(3)	0.522(4)	0.519(3)	0.516(3)	0.518(3)
	occupancy	0.43(1)	0.38(1)	0.43(1)	0.44(1)	0.42(1)
	B_{iso} (Å^2)	7	7	7	7	7
R_{wp} (%)		14.1	13.6	12.2	11.6	11.7
R_{exp} (%)		12.3	11.8	12.6	12.1	12.2
R_{Bragg} (%)		6.41	6.39	4.15	5.16	5.23

goodness of fit, and Figure 2 shows a representative example of fitted diffraction patterns. In Figure 3 are plotted the evolution of the weighed (taking into account oxide sites occupancy) mean (Mo,Cr)−O distance and of the O2 and O3 occupancy rates upon substitution. With the limitation evoked above concerning the accuracy of oxygen positioning, the general trend seems to reflect a progressive decrease of the average distance between the transition metal and its ligands, O2 and O3 sites remaining steadily occupied. Although the average distance appears to decrease more strongly than suggested by the atomic radii (see Table 1) probably due to the inaccuracy in oxygen positioning, such a tendency is in agreement with the cell parameter evolution (see Figure 1). The effect of the substitution of molybdenum by chromium is thus roughly to bring ligands closer to the transition metal without much disturbance in their population. We will see in the next subsection that it is not the case with substitution by tungsten.

3.2. Substitution of Molybdenum by Tungsten.

3.2.1. Cell Parameters. The substitution range of molybdenum is much larger for tungsten than for chromium, namely, up to 80% ($La_2Mo_{0.4}W_{1.6}O_9$).

As $La_2Mo_2O_9$, $La_2Mo_{1.9}W_{0.1}O_9$ is not cubic at room temperature but monoclinic (see Figure 4a). Its subcell parameters have been computed from a full-pattern matching of the X-ray diffraction pattern: $a = 7.1403(3)$ Å, $b = 7.1498(3)$ Å, $c = 7.1553(3)$ Å, $\beta = 89.569(3)°$. The cell volume is surprisingly slightly smaller than that of α-$La_2Mo_2O_9$,[10] but we will see later on that such a feature is not so uncommon in the tungsten series. The splitting is also slightly smaller.

A DTA analysis has been performed on $La_2Mo_{1.9}W_{0.1}O_9$ in order to detect the influence of tungsten substitution on the α/β phase transition (see Figure 4b). The main effect is a significant decrease of the phase transition of about 50 °C relative to $La_2Mo_2O_9$:[1] 580 °C for $La_2Mo_2O_9$ and about 530 °C for $La_2Mo_{1.9}W_{0.1}O_9$. This is consistent with the slightly smaller monoclinic splitting (see above) and the general trend of the β-phase stabilization upon substitution (see below). The thermal peaks upon heating and cooling are broader than those in $La_2Mo_2O_9$,[1] probably due to some heterogeneity in the substitution as already evoked in another phase transition of the system.[7]

Except for this low substitution composition, the other members of the $La_2Mo_{2-y}W_yO_9$ series have a cubic symmetry at room temperature. Figure 1 shows the cubic cell parameter evolution upon substitution, in comparison to that of the Cr series. Contrary to the latter and to other substitution series, the cell parameter evolution upon W substitution is not linear anymore, making this series unique in the whole LAMOX family. Since tungsten ionic radius is slightly larger than that of molybdenum (see Table 1), one would have expected the cell parameter to slightly increase upon W substitution. It is true only up to a substitution range around 50% ($y = 1$).

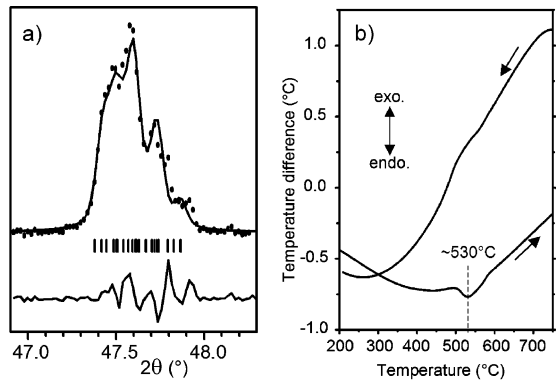

Figure 4. Monoclinic distortion of α-$La_2Mo_{1.9}W_{0.1}O_9$: (a) Splitting of the (123) pseudo cubic X-ray diffraction peak and fit with a monoclinic cell (detail of the full pattern matching). (b) DTA measurement upon heating and cooling showing a thermal peak at the α−β phase transition around 530 °C (heating). Heating/cooling rate = 20 °C/min.

(10) Goutenoire, F.; Isnard, O.; Retoux, R.; Lacorre, P. *Chem. Mater.* **2000**, *12*, 2575.

Above this value, the cell parameter surprisingly decreases, in a way that mimics the decrease observed for chromium (it gives the impression that both series have the same limits in term of lower cell volume, but it does not appear to be a general steric rule[2,11]). Such a singular evolution cannot be ascribed to some reduction in the tungsten valence since all samples have been prepared in air and are creamy white in color. Although the cell parameter variations are not very large (less than 0.02 Å in the whole ranges) compared to those of other members of the LAMOX family,[2] they are indeed significant and definitely well beyond the precision of the used diffractometers. Tungsten-substituted LAMOX being the most promising members of the family because of the stabilizing effect of W against reducibility, we have decided to carry out a detailed study of the structural effects at stake in the series.

The unusual evolution of cell parameters gives first clues. The linear variation of cell parameters as a function of substitution rate in the chromium series is a direct consequence of the linear variation of the average ionic radius of hexavalent species. It allows us to use it as a reference in order to correlate the cell parameter and the hexavalent ionic radius in this structural type, a trivial multiplier coefficient being deduced from the slopes of both linear variations. Table 1 lists the ionic radii of hexavalent Cr, Mo, and W ions in their most frequent coordination states.[12] Interestingly enough, within the accuracy of available data, the radius variation from one element to its neighbor appears to be independent from the coordination number (−0.15 Å from Mo^{6+} to Cr^{6+}, +0.01 Å from Mo^{6+} to W^{6+}), which suggests an absolute reference whatever the coordination. It means that, for any given coordination, the average ionic radius—and hence the cell parameter—should vary 15 times less for tungsten substitution than for chromium substitution, with opposite sign of the variation.

Such a variation for tungsten substitution is plotted on Figure 1 as a dashed line. As a rough—and probably not very realistic—estimate of the influence of coordination number, an equivalent variation assuming a smaller ionic radius for tungsten resulting from a smaller (−1) coordination number than for Mo is also reported (dotted line). Clearly the observed variation follows almost exactly the expected dashed line trend up to 50% substitution, which validates the above analysis (same oxidation states and linear dependence of cell parameter on ionic radius). Above 50% W, however, the observed cell parameters deviate significantly from the expected line and tend to join the dotted line. Our interpretation of this behavior is that when tungsten becomes predominant, it imposes a change in the hexavalent cation ligand sphere toward a lower coordination. Such an interpretation has of course to be validated by a detailed structural analysis, and that is what we attempt next.

3.2.2. Crystal Structure. The neutron diffractograms were used to refine the crystal structure of the $La_2Mo_{2-y}W_yO_9$ series. All patterns exhibit a strong undulation of the background as a contribution of local static structural disorder

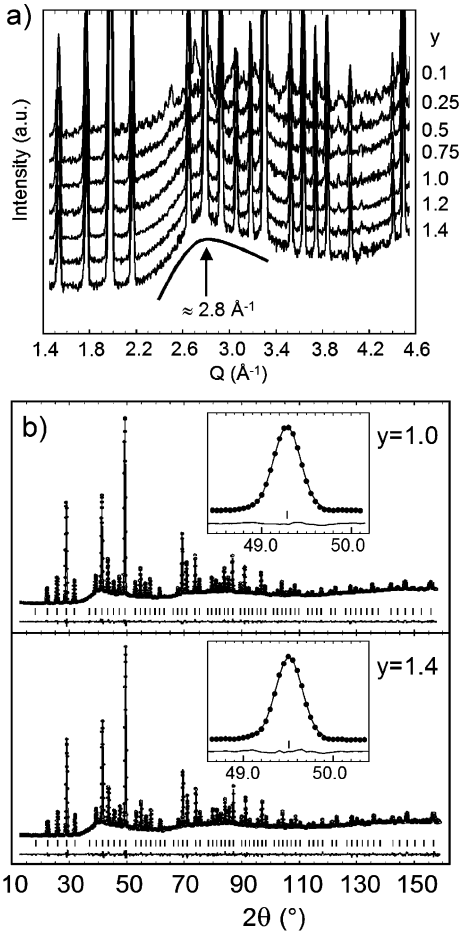

Figure 5. Neutron diffraction patterns of $La_2Mo_{2-y}W_yO_9$: (a) Modulation of the neutron diffraction background along the series showing a first maximum around 2.8 $Å^{-1}$ (see text for details). (b) Observed (dots), calculated (lines), and difference (below) patterns for La_2MoWO_9 (upper) and $La_2Mo_{0.6}W_{1.4}O_9$ (lower) using the structural models in Table 3. In insert: the (123) cubic peak (main neutron reflection line).

to the elastic diffuse scattering.[13] Such a feature has already been noticed in other oxide-ion conductors[14,15] as well as in the α form of $La_2Mo_2O_9$[10] and is interpreted as originating from some structural static disorder on the oxygen sublattice. Tungsten substitution does not modify substantially the magnitude of the background modulation nor its structure (see Figure 5a). However, the smaller number of (usually intense) diffraction peaks makes it easier to estimate the Q-position of the first undulation maximum, when compared to that observed in α-$La_2Mo_2O_9$ where small superstructure peaks are superimposed (see Figure 2 in ref 10). It can be clearly seen in Figure 5a that this maximum is close to $Q_{max} = 2.8$ $Å^{-1}$. According to the Debye formula, the preferred pair distance characteristic of the short-range order can be deduced from this first marked maximum as $d_m = (2\pi \times 1.23)/Q_{max}$,[15] which gives in our case $d_m \approx 2.76$ Å. This is typically characteristic of mean O−O distances in the ligand environment of cations, thus confirming that the observed

(11) Georges, S.; Goutenoire, F.; Altorfer, F.; Sheptyakov, D.; Fauth, F.; Suard, E.; Lacorre, P. *Solid State Ionics* **2003**, *161*, 231.
(12) Shannon, R. D. *Acta Crystallogr. Sect. A* **1976**, *32*, 751.
(13) Fender, B. E. F. In *Chemical Applications of Thermal Neutron Scattering*; Willis, B. T. M., Ed.; Oxford University Press: London, 1974; pp 250−270.
(14) Aldebert, P.; Dianoux, A. J.; Traverse, J. P. *J. Phys. (Paris)* **1979**, *40*, 1005.
(15) Vannier, R. N.; Abraham, F.; Nowogrocki, G.; Mairesse, G *J. Solid State Chem.* **1999**, *142*, 294.

Table 3. Refined Crystal Structure Parameters (Space Group $P2_13$) in the Series $La_2Mo_{2-y}W_yO_9$ from Neutron Powder Diffraction Data

y		0.25	0.5	0.75	1	1.2	1.4
a (Å)		7.1547(1)	7.1549(1)	7.1540(1)	7.1506(1)	7.1459(1)	7.1408(1)
La (4a)	x	0.8544(2)	0.8544(2)	0.8545(2)	0.8544(2)	0.8549(2)	0.8554(2)
	occupancy	1	1	1	1	1	1
	B_{eq} (Å^2)	4.4(1)	4.6(1)	4.4(1)	4.5(1)	4.5(1)	4.2(1)
Mo/W (4a)	x	0.1677(5)	0.1657(4)	0.1664(4)	0.1655(3)	0.1646(4)	0.1649(4)
	occupancy	0.875/0.125	0.75/0.25	0.625/0.375	0.5/0.5	0.4/0.6	0.3/0.7
	B_{eq} (Å^2)	4.2(1)	4.5(1)	4.8(1)	4.8(1)	5.0(1)	5.1(1)
O1 (4a)	x	0.3129(5)	0.3093(4)	0.3094(4)	0.3082(2)	0.3081(3)	0.3082(3)
	occupancy	1	1	1	1	1	1
	B_{eq} (Å^2)	5.9(1)	5.8(1)	6.0(2)	5.8(1)	6.0(1)	5.9(1)
O2 (12b)	x	0.9922(5)	0.9948(4)	0.9946(5)	0.9952(3)	0.9938(4)	0.9923(5)
	y	0.1809(9)	0.1729(9)	0.174(1)	0.1719(6)	0.1734(8)	0.1744(9)
	z	0.3473(8)	0.3454(7)	0.3463(8)	0.3464(5)	0.3461(6)	0.3474(7)
	occupancy	0.72(1)	0.67(1)	0.69(1)	0.66(1)	0.65(1)	0.63(1)
	B_{eq} (Å^2)	6.0(2)	6.3(3)	6.5(3)	6.4(2)	6.0(2)	5.8(3)
O3 (12b)	x	0.906(2)	0.880(1)	0.882(1)	0.8802(8)	0.880(1)	0.884(2)
	y	0.646(4)	0.615(3)	0.613(3)	0.614(2)	0.614(3)	0.625(3)
	z	0.559(1)	0.5607(8)	0.5588(8)	0.5614(6)	0.5624(7)	0.5639(8)
	occupancy	0.44(1)	0.49(1)	0.48(1)	0.50(1)	0.51(1)	0.53(1)
	B_{eq} (Å^2)	19(2)	34(2)	35(2)	35(1)	34(2)	36(2)
R_{wp} (%)		12.00	10.30	11.40	8.58	9.80	12.50
R_{exp} (%)		10.32	7.97	9.74	5.61	7.58	10.83
R_{Bragg} (%)		2.72	2.81	2.60	2.34	2.66	3.03

static disordering concerns mainly oxide ions. It is also consistent with the fact that the background modulation is clearly visible in neutron and not in X-ray diffraction patterns. To be correlated with this anionic static disordering are the oxide-ion conductivity properties of these materials, as well as the random substitution on the hexavalent cationic sublattice.

The crystal structure of six members of the $La_2Mo_{2-y}W_yO_9$ series ($x = 0.25, 0.5, 0.75, 1.0, 1.2, 1.4$) has been refined from neutron diffraction data using the high-temperature cubic structure of β-$La_2Mo_2O_9$ as a starting model.[11] Then successively the structure of one compound with low-W content was used as a starting model for that of a higher-W content one. For each refinement, the background was pointed between diffraction lines of space group $P2_13$, with the calculated counts at these points allowed to be refined. As in previous studies,[10,11] anisotropic thermal parameters were refined. Our expectation was, despite a relatively low ratio between the effective number of reflections and the number of intensity-related refined parameters (around 2.3), to detect trends on atomic parameters (including oxide ions, hence the use of neutron diffractograms) reliable enough to be significant. Table 3 gives the main results of the refinements. The quality of fit was equal all along the series, as can be seen on selected profiles in Figure 5b.

We have now to closely examine the incidence of tungsten substitution on the atomic positions, especially of oxide ions. The ligand arrangement around cations in β-$La_2Mo_2O_9$ is not straightforward to describe.[10,11] Seven oxygen positions surround the hexavalent cation: three are located in the same plane as the cation (O2 site), while three others are on one side of the previous triangle (O3 site) and the remaining one on the other side (O1 site). The coordination sphere of hexavalent cations thus looks like a triangular bipyramid, one of the corners being split in 3 positions around the 3-fold axis (see dotted part of Figure 10). O2 and O3 sites are more or less partially occupied with large anisotropic thermal factors reflecting oxygen delocalization (probably in connection with anionic transport). The closest oxygen site is O3, sites O1 and O2 being farther away. Given the error bars, no clear evolution of these M^{6+}−O interatomic distances with W substitution is evidenced (see Figure 6a). This is in apparent contradiction with our previous analysis based on

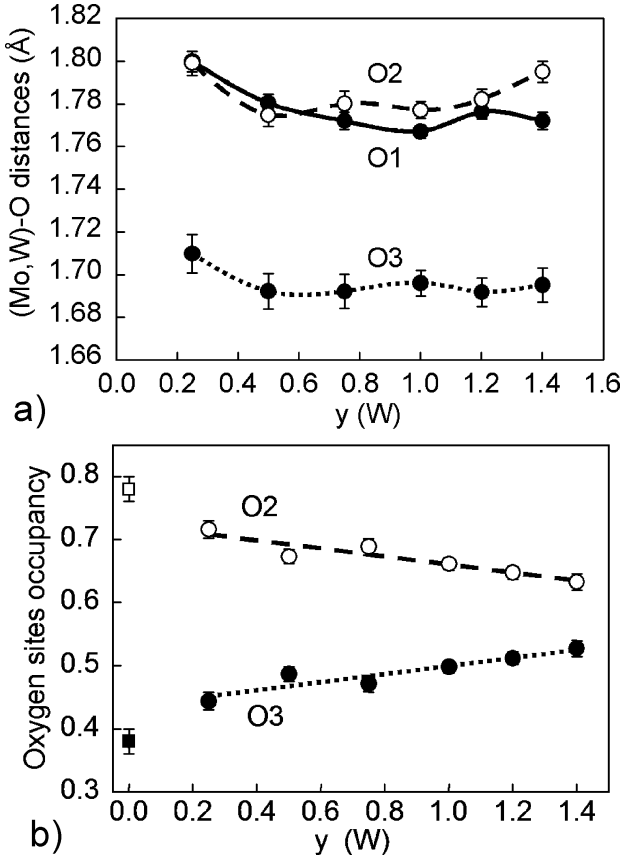

Figure 6. Evolution, with tungsten content *y*, of the (Mo,W)−O distances (a) and of O2 and O3 oxygen sites occupancy (b) in $La_2Mo_{2-y}W_yO_9$. As a comparison, the site occupancies in β-$La_2Mo_2O_9$ at 670 °C are indicated (square symbols, from ref 11).

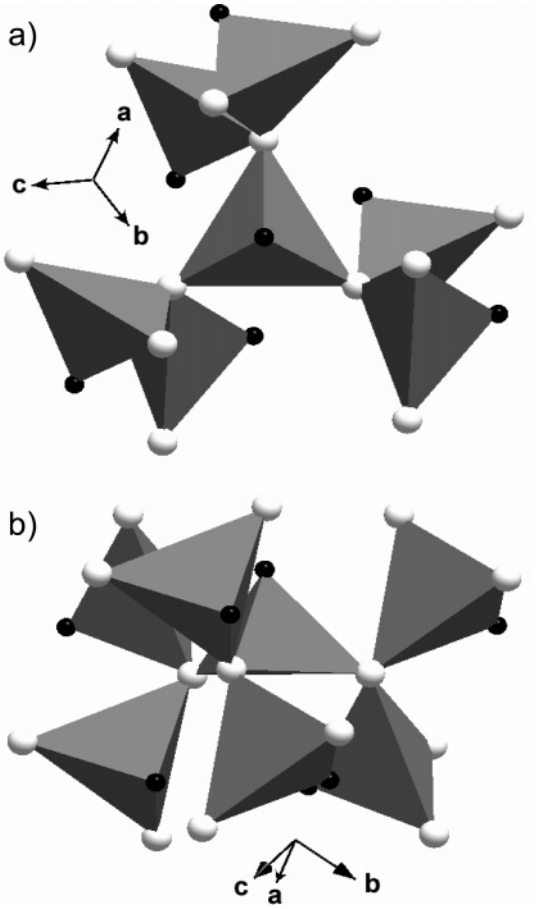

Figure 7. A [O1La_3Mo] tetrahedral unit of the β-type LAMOX and its six neighbors, projected along the 3-fold axis of the structure (a) and perpendicular to it (b). Black spheres = Mo^{6+} or substitute, white spheres = La^{3+} or substitute.

cell parameters (in section 3.2.1). Only a closer examination of oxygen site occupations gives better insight (see Figure 6b). As a matter of fact, there appears to be a non-negligible modification in O2 and O3 site occupations upon substitution, the population of the two sites tending to re-equilibrate for higher tungsten contents. It means that O3 sites (closest to hexavalent cations) become more populated, at the expense of farther away O2 sites. It confirms that a change induced by tungsten substitution occurs in the coordination sphere of hexavalent ions, which corresponds to a decrease in the average hexavalent cation coordination. This is finally consistent with our previous assumption based on the peculiar evolution of the cell parameter (see section 3.2.1). However, the rather smooth and monotonic change in oxygen site occupation does not explain the nonlinear variation of the cell volume. Therefore, a deeper structural analysis has to be carried out.

For this purpose we introduce another type of structural representation, different from the conventional representation in terms of coordination polyhedra of cations described previously.[11] It is inspired from the alternative approach of O'Keeffe and Hyde[16] who, in an inversion of the traditional approach, put emphasis on the coordination sphere of anions. Two types of anion surroundings coexist in the β-$La_2Mo_2O_9$ crystal structure. Site O1 is surrounded by 4 cations (1Mo + 3La) forming a tetrahedron and sites O2 and O3 by 3 cations (1Mo + 2La) forming distorted triangles.[17] Given its closed tetrahedral surrounding, the fully occupied O1 site is the least likely to be concerned with oxide ion conduction, when compared to O2 and O3 sites with opened triangular surroundings. This is consistent with both the LPS (Lone Pair Substitution) concept[18] and the charge carrier concentration (around 3 oxide ions per formula unit) determined through tracer diffusion coefficient measurements[19] and interpreted as involving mostly O3 and partly O2 sites, both being partially occupied. A rigid structural framework built up from [O1La3Mo] tetrahedral units surrounded by partly delocalized oxide ions on O2 and O3 sites is therefore more likely to reflect the basic nature of the β-$La_2Mo_2O_9$ crystal structure and transport properties.

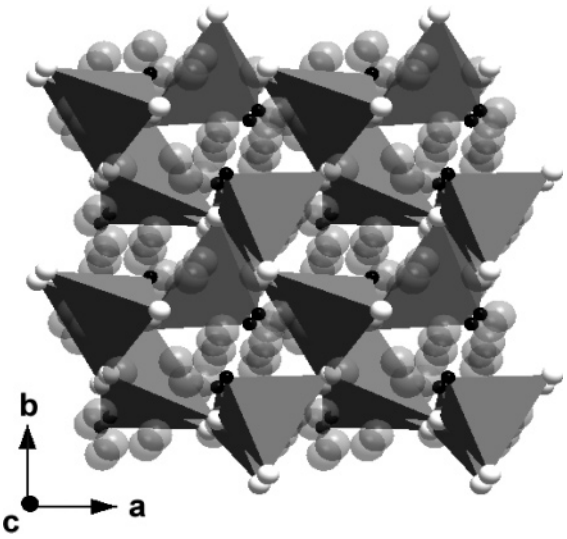

Figure 8. New description of the β-$La_2Mo_2O_9$ structural type formulated as $[OLaMo]_2O_7$, with a [OLaMo] framework and O2 and O3 oxide ions sites embedded in its tunnels. Black spheres = Mo^{6+} or substitute, white spheres = La^{3+} or substitute, transparent gray spheres = O2 and O3 oxide ion sites.

Figure 7 shows one of these [O1La_3Mo] tetrahedral units and its neighbors. The Mo corner is terminal, but every unit shares each of its three La corners with two other units of the same kind, thus forming a three-dimensional extension, resulting in a $OLa_{3/3}Mo$ = [OLaMo] framework. Adding the extra O2 and O3 oxide ions leads to a reformulation of $La_2Mo_2O_9$ as $[OLaMo]_2O_7$, or $[OLaMo]_2O_7\square$ if we take into account the vacancy $\square$ derived from the LPS concept.[18] Figure 8 shows a representation of the full structure according to this alternative description. The [OLaMo] framework shapes tunnels along the cubic cell axes, in which oxide ions on sites O2 and O3 are located (transparent spheres in Figure 8). Partial occupancy of these sites and large anisotropic thermal factors related to atomic delocalization allow for short O3−O3 and O2−O3 distances (<2.2 Å), favorable to intra- and intersite jumps: they define a 3D extension of possible conduction paths within the [OLaMo] rigid framework.

(16) O'Keeffe M.; Hyde, B. G. *Struct. Bonding* **1985**, *61*, 77.
(17) Emery, J.; Massiot, D.; Lacorre, P.; Laligant, Y.; Conder, K. *Magn. Res. Chem.* **2005**, *43*, 366.
(18) Lacorre, P. *Solid State Sci.* **2000**, *2*, 755.
(19) Georges, S.; Skinner, S. J.; Steil, M. C.; Lacorre, P. *J. Chem. Soc., Dalton Trans.* **2004**, *19*, 3101.

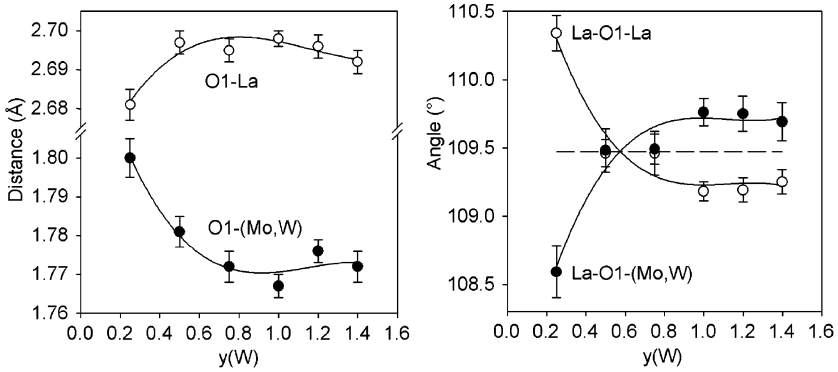

Figure 9. Evolution upon substitution of interatomic distances (a) and angles (b) within the inverse tetrahedral units of $La_2Mo_{2-y}W_yO_9$. The full lines are third-order regression fits to the structural data as refined from neutron diffraction patterns, and the dashed horizontal line corresponds to the ideal angle at the center of a regular tetrahedron (109.47°).

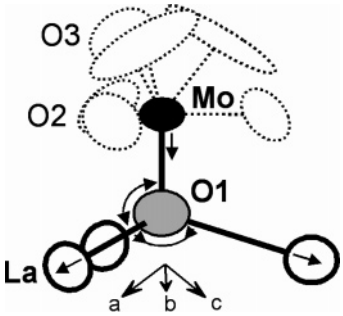

Figure 10. Atomic shifts and rotations within the inverse tetrahedral units of β-$La_2Mo_2O_9$ upon increasing substitution (up to $y = 1$ in $La_2Mo_{2-y}W_yO_9$). The oxygen environment of molybdenum in terms of partially occupied O2 and O3 sites with large anisotropic thermal factors (dotted) is also represented (at 670 °C, from ref 11).

Since we already have analyzed previously the modification induced on O2 and O3 sites, let us now focus on the effect of W substitution on the [O1LaMo] framework. Figure 9 shows the evolution upon substitution of interatomic distances and angles within [O1La_3Mo] tetrahedral units. Clear non-monotonic behavior is observed that can be paralleled to that of the cell parameter (see Figure 1). Below $y = 1$, larger O1−La distances increase, whereas the shorter O1−(Mo,W) distance decreases with y, which is somewhat surprising given the larger size of tungsten ion. Conversely, tetrahedral angles at the oxide ion central position become more regular. Figure 10 summarizes the tetrahedral distortion upon substitution below $y = 1$. Above $y = 1$, a leveling off is observed, with a fainter tendency to reverse evolutions in the anion−cation distances.

The above detailed structural analysis shows that the peculiar cell volume variation upon tungsten substitution for molybdenum in $La_2Mo_2O_9$ has two main origins: a nonlinear evolution of the geometry of [O1La_3(Mo,W)] antitetrahedral units, combined with a smooth variation in O2/O3 site occupation resulting in a decrease.

4. Conclusion

In this paper we have presented a study of the influence of chromium and tungsten substitutions on the structural arrangement of fast oxide-ion conductor $La_2Mo_2O_9$. Whereas substitution by chromium appears to have little incidence on the structural arrangement, apart from a regular shrinkage of the cell volume due to substitution by a smaller cation, substitution by tungsten has a more complex, nonlinear effect: first, a slight regular increase (W:Mo < 1) and then a more abrupt decrease (W:Mo > 1) of the cell volume as a function of W content. Although inhomogeneous repartition of tungsten and/or metastable distribution of oxide ions cannot be totally ruled out, this singular evolution has been correlated with nonlinear changes in the O1 site surrounding and a variation in O2/O3 site occupation resulting in/from a decrease of the coordination number of tungsten ions. Such a modification in the distribution of conducting oxide ions is likely to have an incidence on the transport mechanism of the materials, which will be studied in a forthcoming paper. Besides, a new description of the β-$La_2Mo_2O_9$ structural type has been proposed, which hopefully provides a better way to analyze the transport properties of this family of fast oxide-ion conductors.

Supporting Information Available: CIF files for $La_2Mo_{1.75}W_{0.25}O_9$, $La_2Mo_{1.5}W_{0.5}O_9$, $La_2Mo_{1.25}W_{0.75}O_9$, La_2MoWO_9, $La_2Mo_{0.8}W_{1.2}O_9$, and $La_2Mo_{0.6}W_{1.4}O_9$. This material is available free of charge via the Internet at http://pubs.acs.org.

CM0501214